



Wilks, M., Ayele, A., Kendall, J-M., & Wookey, J. (2017). The 24th January 2016 Hawassa earthquake: implications for seismic hazard in the Main Ethiopian Rift. *Journal of African Earth Sciences*, 125, 118-125. <https://doi.org/10.1016/j.jafrearsci.2016.11.007>

Peer reviewed version

Link to published version (if available):  
[10.1016/j.jafrearsci.2016.11.007](https://doi.org/10.1016/j.jafrearsci.2016.11.007)

[Link to publication record in Explore Bristol Research](#)  
PDF-document

This is the author accepted manuscript (AAM). The final published version (version of record) is available online via Elsevier at <http://www.sciencedirect.com/science/article/pii/S1464343X16303569>. Please refer to any applicable terms of use of the publisher.

## University of Bristol - Explore Bristol Research

### General rights

This document is made available in accordance with publisher policies. Please cite only the published version using the reference above. Full terms of use are available:  
<http://www.bristol.ac.uk/red/research-policy/pure/user-guides/ebr-terms/>

1   **Title:**

2   The 24th January 2016 Hawassa Earthquake: Implications for Seismic Hazard in the Main  
3   Ethiopian Rift.

4  
5   **Authors:**

6   Matthew Wilks<sup>a</sup>, Atalay Ayele<sup>b</sup>, J-Michael Kendall<sup>a</sup> & James Wookey<sup>a</sup>.  
7  
8

9   **Affiliations:**

10   a. School of Earth Sciences, University of Bristol, Wills Memorial Building, Queens Road,  
11   Bristol, UK. BS8 1RJ.

12   b. Institute of Geophysics, Space Science, and Astronomy, Addis Ababa University,  
13   Addis Ababa, Ethiopia.  
14

15   **Contact Details:**

16   Matthew Wilks

17   Email: [Matt.Wilks@bristol.ac.uk](mailto:Matt.Wilks@bristol.ac.uk)

18   Tel: +44 (0) 117 954 5400

19   Fax: +44 (0)117 954 5420

20   Mob: +44 (0) 7817 256068

## Abstract

Earthquakes of low to intermediate magnitudes are a commonly observed feature of continental rifting and particularly in regions of Quaternary to Recent volcanism such as in the Main Ethiopian Rift (MER). Although the seismic hazard is estimated to be less in the Hawassa region of the MER than further north and south, a significant earthquake occurred on the 24th January 2016 in the Hawassa caldera basin and close to the Corbetti volcanic complex. The event was felt up to 100 km away and caused structural damage and public anxiety in the city of Hawassa itself. In this paper we first refine the earthquake's location using data from global network and Ethiopian network stations. The resulting location is at 7.0404°N, 38.3478°E and at 4.55 km depth, which suggests that the event occurred on structures associated with the caldera collapse of the Hawassa caldera in the early Pleistocene and not through volcano-tectonic processes at Corbetti. We calculate local and moment magnitudes, which are magnitude scales more appropriate at regional hypocentral distances than ( $m_b$ ) at four stations. This is done using a local scale (attenuation term) previously determined for the MER and spectral analysis for  $M_L$  and  $M_W$  respectively and gives magnitude estimates of 4.68 and 4.29. The event indicates predominantly normal slip on a N-S striking fault structure, which suggests that slip continues to occur on Wonji faults that have exploited weaknesses inherited from the preceding caldera collapse. These results and two previous earthquakes in the Hawassa caldera of  $M > 5$  highlight that earthquakes continue to pose a risk to structures within the caldera basin. With this in mind, it is suggested that enhanced monitoring and public outreach should be considered.

**Key Words:** Main Ethiopian Rift, Seismic Hazard, Ethiopia, Seismicity and Tectonics, Continental Tectonics, Earthquake Magnitudes.

# 1. Introduction

The Main Ethiopian Rift (MER) is a magmatic rift that marks the axis of continental extension between the Nubian and Somalian plates. It represents the portion of the greater East African Rift System that traverses through Ethiopia and is characterised by numerous magmatic segments and volcanic centres that have assisted in accommodating extensional strain since ~2 Ma (Ebinger & Casey, 2001; Casey et al., 2006). Seismicity in the MER is generally diffuse along the rift basin (Fig. 1), where earthquakes are typically of small to intermediate magnitudes ( $M < 6$ ). However, numerous examples of structurally damaging events have been documented over the past century, such as:

- A  $M_{6.3}$  event close to Hawassa in 1960 that was felt 200 km away and produced 28 aftershocks (Gouin, 1979).
- A  $M_W 5.3$  earthquake on the eastern escarpment of the Hawassa basin in 1983 that caused a rock slide and building collapse in Wendo Genet (Hofstetter & Beyth, 2003).
- A  $m_b 4.8$  earthquake in 1985 that was strongly felt at Lake Langano, cracking hotels and buildings around the resort (Asfaw, 1998).
- A pair of events ( $m_b > 4.1$ ) on consecutive days in 1993 in the northern CMER, the second of which, caused damage in Nazret (Asfaw, 1998)
- A  $M_W 5.0$  event at Chabbi in 1995 (Hofstetter & Beyth, 2003).

Despite improved monitoring over the past decades however, seismic hazard remains relatively poorly constrained (Midzi et al., 1999).

On the 24th January 2016 at 18:34:35.590 UTC (21:34 local time), an earthquake occurred in the Hawassa region that was felt up to 100 km away, including the major towns and cities of Hawassa (pop. 165 275, [2012]), Shashemene (pop. 122 046, [2012]) and Dila (pop. 79 892, [2012]) (Fantahun, 2016). A series of further tremors were also reported, causing minor structural damage in Hawassa as well as scattered power outages. Although no injuries were reported as a direct consequence of the event, around 100 students at Hawassa University required treatment when a stampede ensued as they tried to flee their dormitories. Some residents were apprehensive in returning to their homes and chose to sleep outside in fear of building collapse.

The earthquake was recorded by both the National Earthquake Information Center (NEIC) and the Centre Sismologique Euro-Méditerranéen (CSEM), who both estimated a body-wave magnitude ( $m_b$ ) of 4.4. The NEIC located the event beneath the city of Hawassa at  $7.088^\circ\text{N} \pm 8.8 \text{ km}$ ,  $38.479^\circ\text{E} \pm 8.8 \text{ km}$  and at a depth of  $10 \pm 2.0 \text{ km}$  below sea level (National Earthquake Information Center [NEIC], 2016), while the CSEM located it to the southwest of Corbetti, at  $6.98^\circ\text{N} \pm 6.6 \text{ km}$ ,  $38.19^\circ\text{E} \pm 13.7 \text{ km}$  using a fixed depth of 10 km (International Seismological Centre, 2016) (Fig. 2b).

The MER is subdivided into three segments: the northern, central and southern MER, which exhibit the progressively maturing stages of continental rifting from initial break-up, from south-to-north (Mohr, 1967; Hayward & Ebinger, 1996; Ebinger, 2005). In the early development of the MER, extensional strain was accommodated by long, widely-spaced border faults that bounded the margins of the rift (Fig. 2b), showing general trends of  $\sim N30^\circ E$  in the CMER and  $\sim N-S$  in the SMER.

At  $\sim 2$  Ma the style of deformation switched considerably in the CMER with the boundary faults becoming relatively inactive (Wolfenden et al., 2004; Casey et al., 2006; Keir et al., 2006a). Deformation became concentrated along relatively short ( $< 20$  km), finely spaced ( $> 2$  km) faults towards the rift axis at the Wonji Fault Belt (WFB) (Chorowicz et al., 1994; Boccaletti et al., 1998; Ebinger & Casey, 2001). These faults trend obliquely to the border faults at  $\sim N12^\circ E$  and formed concurrently with a focusing of volcanism towards the centre of the rift (Agostini et al., 2011). Around the latitude of the 2016 event is the boundary between the CMER and SMER, where the rift's margins rotate from  $N020-035^\circ E$  to  $N005-020^\circ E$  and where magmatic processes play a lesser role in accommodating extensional strain to the south (Bonini et al., 2005).

The Hawassa caldera basin is located in this region at the eastern escarpment of the rift, forming a topographic depression of  $35 \times 20$  km that is elongated  $\sim E-W$ . The basin is characterised by silicic lava flows, pumices and welded tuffs, which are dated at 1.85–1.1 Ma (WoldeGabriel et al., 1990). More recent volcanism has resulted in the formation of the Corbetti volcanic centre at the northwestern edge of the Hawassa caldera, where rhyolitic lava flows accumulated and initiated a caldera collapse event at  $175 \pm 20$  ka (Hutchison, 2015). Satellite imaging has shown significant surface deformation ( $< 14$  cm) at Corbetti over the past twenty years (Biggs et al., 2011), while the volcano has also been outlined as a geothermal energy resource of vast potential (Kebede, 2014).

In this paper we present this widely-felt, significant event as an example of the potential seismic risk in the region surrounding the Hawassa caldera. The event received public attention across Ethiopia, making it unusual as estimations of hazard are lower at this latitude than elsewhere in the rift (Fig. 1). We therefore locate the earthquake ourselves to refine the contrasting locations suggested by the NEIC and CSEM and determine local ( $M_L$ ) and moment ( $M_W$ ) magnitudes, which are magnitude scales more appropriate for data recorded at regional distances than  $m_b$ . We then compute a focal mechanism using P-wave polarities to investigate the mode of faulting for the event.

## 2. Earthquake Location

To locate the earthquake, we manually pick P-arrivals on data recorded at seven stations belonging to the GSN (FURI, KMBO, MBAR, RAYN and UOSS) and GEOFON

(LODK and KIBK) (Fig. 2a). These traveltime picks are supplemented by P- and S-wave picks from 5 stations from the Ethiopian Seismic Network (EH) at DESE, ANKE, AAE, WERA and DILA. With large hypocentral offsets of up to  $24.95^\circ$  between the source location and furthest receivers, we calculate P- and S-wave arrival times using the ak135 global model (Kennett et al., 1995) and perform the location in NONLINLOC's 'global mode' (Lomax et al., 2000). In this approach, the optimal hypocentre is searched for in a spherical Earth that spans the uppermost 50 km of the crust and the upper mantle (Lomax et al., 2009).

The resulting best-fit location is at  $7.0404^\circ$ ,  $38.3478^\circ$ , which is in between those reported by the NEIC and CSEM (Fig. 2b). This places the event on the western rim of the Hawassa caldera and may be indicative of faulting associated with structures that formed during caldera collapse (WoldeGabriel et al., 1990). In depth, the earthquake appears shallower than the reported locations of 10.0 km at 4.55 km. The one standard deviation uncertainty ellipsoid corresponds to uncertainties of 1.79, 8.10 and 3.4 km in latitude, longitude and depth respectively (2.70, 12.19 and 5.12 km to 95% confidence). The relatively poorer location constraints in longitude can be ascribed to the lack of recording stations to the east and west of the event.

### 3. Magnitudes

Body-wave magnitude is a commonly used empirical magnitude scale used for teleseismic earthquakes (Gutenberg & Richter, 1956). It is calculated using the maximum amplitude of the P-wave, when recorded on a short period seismograph, and a correcting term for attenuation. Estimates of  $m_b$  were provided by the NEIC and CSEM of 4.4 for the Hawassa event. However, at epicentral distances less than  $10\text{--}15^\circ$  the correction function is highly variable with distance and depth due to the heterogeneity of the crust and upper mantle (Bormann et al., 2013). Consequently, it is recommended that only epicentral distances greater than  $20^\circ$  should be considered when calculating  $m_b$ . We therefore derive local and moment magnitudes using four stations (FURI, LODK, KIBK and KMBO) with epicentral distances of  $198\text{--}1050$  km ( $1.78\text{--}9.43^\circ$ ), where picks for both P- and S-wave arrivals are possible.

#### 3.1. Local Magnitude

For local magnitude we use the attenuation term defined for the Main Ethiopian Rift by Keir et al. (2006b). Surface wave energy is suppressed automatically by the convolution of the instrument response to a Wood-Anderson seismograph, which acts as a high-pass filter above 2 Hz (Havskov & Ottemoller, 2010). We measure the maximum peak-to-peak amplitude displacements on each horizontal component (Fig. 3) and halve them to estimate the zero-to-peak amplitudes ( $A_{WA}$ ). We then evaluate:  $M_L = \log A_{WA} + 1.196997 \log(r/17) + 0.001066(r - 17) + 2.0$ , where  $r$  is the hypocentral distance in km, and average across the two values at each station. This computes magnitudes of 4.68, 4.31, 4.88 and 4.85 for stations FURI, LODK, KMBO and KIBK respectively

(Table 1). The variability in these values may reflect our inability to apply station corrections to this single event but from these values we calculate the mean and determine an overall  $M_L$  estimate of  $4.68 \pm 0.27$ . The uncertainty is the standard deviation of the magnitudes determined on each component of each station.

| Station | Distance<br>(km) | Comp | M <sub>L</sub> | $\bar{M}_L$ |
|---------|------------------|------|----------------|-------------|
| FURI    | 198              | N    | 4.74           | 4.68        |
|         |                  | E    | 4.62           |             |
| LODK    | 531              | N    | 4.28           | 4.31        |
|         |                  | E    | 4.32           |             |
| KMBO    | 922              | N    | 4.85           | 4.88        |
|         |                  | E    | 4.90           |             |
| KIBK    | 1050             | N    | 5.06           | 4.85        |
|         |                  | E    | 4.65           |             |
|         |                  |      |                | 4.68 ± 0.27 |

Table 1:  $M_L$  results for the Hawassa earthquake using the Keir et al. (2006b) attenuation term for the MER at four stations.

### 3.2. Moment Magnitude

Spectral analysis is performed to determine  $M_W$  by first convolving the raw seismograms to displacement using the appropriate poles and zeros. We compute the frequency spectra of seismograms rotated to the ray-frame for P-, SV- and SH-wave arrivals and the background noise prior to the onset of the P-wave in each case. We then subtract the noise spectra from the spectra of the seismic arrivals and fit the resulting spectra with a Brune source model (Brune, 1970) in a least- squares sense. In this method the spectral amplitude of the low frequency signal ( $\Omega_0$ ), corner frequency ( $f_c$ ) and seismic quality factor ( $Q$ ) are solved for simultaneously and we adjust the frequency band at which the spectra is fitted (aiming to keep it as wide as possible) to achieve the best estimate of the source parameters. Where convergence is achieved in all three parameters, the seismic moment ( $M_0$ ) is determined via:

$$M_0 = \frac{4\pi\rho v^3 \Omega_0}{R \times F \times G(\Delta, h)},$$

where  $\rho$  and  $v$  are the densities ( $2790 \text{ kg/m}^3$ ) and seismic wave velocities ( $5.99 \text{ km/s}$  for P-waves and  $3.53 \text{ km/s}$  for S-waves) at the source respectively.  $R$  and  $F$  are constants pertaining to the radiation pattern and free surface effects as derived by Aki & Richards (2002), where values for the  $R$  coefficients are calculated for P- and SV- and SH-waves subject to the focal mechanism computed in the following and  $F$  is set equal to 2.0. For P-waves we use the geometrical spreading relationship:  $G(\Delta, h) = 1/r$

where ( $\Delta$ ) is epicentral distance and  $h$  is focal depth and for S-waves we assume:  
 $G(\Delta, h) = 1/\sqrt{\Delta\Delta_0}$ , where  $\Delta_0$  is a reference distance that assumes surface wave  
dispersion at large hypocentral distances (Havskov & Ottemoller, 2010). This is set to  
100 km after Herrmann & Kijko (1983). The moment magnitude  $M_W$  is then calculated  
via the expression:  $M_W = \frac{2}{3}\log(M_0) - 6.07$ .

The spectral fitting on each component of the four stations and the output parameters  
in each case are presented in Fig. 4 and Table 2 respectively. At FURI, the spectra are  
fit accurately at frequencies greater than 0.6 Hz on all components and the observed  
spectral levels are well constrained. The determined values of  $\Omega_0$ ,  $f_c$  and  $Q$  correspond  
to magnitudes ranging between 4.07 and 4.63 that produces an overall estimate of 4.29  
for the station. Good fits are also achieved at LODK at frequencies greater than 0.8 Hz,  
although the signal to noise ratio is noticeably higher in the P-wave spectra. The  
parameters produce a magnitude estimate of 4.15.

At KMBO, the signal to noise ratio is reduced below 0.8 Hz and above 6 Hz, which  
hinders the spectral fitting below and above these frequencies. Between these  
frequencies, convergence in corner frequency is not possible in the P- and SV-wave  
spectra and these results are omitted. The SH-spectra produces a magnitude estimate of  
3.64 although the spectral amplitudes below 0.5 Hz appear greater than that determined  
in the  $\Omega_0$  fitting. A high noise level above 6 Hz is also evident at KIBK that in the P-  
wave spectra produces a particularly poor fit. The corner frequency fails to converge as a  
consequence and the component is excluded. Good fits are achieved in the SV- and  
SH-wave spectra however, which define a magnitude of 4.15 at the station.

Taking the values from each component where the source model is constrained produces  
an overall averaged estimate of the seismic moment equal to  $3.00 \times 10^{15}$  N m and a  
magnitude of  $4.14 \pm 0.26$ . However, the greater epicentral distances of 531, 933 and 1050  
km at LODK, KMBO and KIBK and the relatively poor spectral fits to those at FURI,  
imply that the derived spectral amplitudes may be underestimated at these stations. We  
therefore suggest that only the value from FURI should be considered in determining  
 $M_W$ . In this case the revised  $M_0$  release of the event is  $5.04 \times 10^{15}$  N m and  $M_W$  is equal  
to  $4.29 \pm 0.30$ .



| Station | Comp | Freq Range (Hz) | $\Omega_0$ (nm)    | $f_c$ (Hz) | Q   | $M_0$ (Nm)            | $M_W$ | $\bar{M}_W$ |
|---------|------|-----------------|--------------------|------------|-----|-----------------------|-------|-------------|
| FURI    | P    | 0.6–9           | $1.50 \times 10^3$ | 2.61       | 209 | $1.12 \times 10^{16}$ | 4.63  | 4.29        |
|         | SV   | 0.5–9           | $6.80 \times 10^3$ | 2.01       | 255 | $2.30 \times 10^{15}$ | 4.17  |             |
|         | SH   | 0.6–9           | $1.14 \times 10^4$ | 2.03       | 173 | $1.63 \times 10^{15}$ | 4.07  |             |
| LODK    | P    | 0.7–8           | $4.69 \times 10^2$ | 4.12       | 330 | $1.82 \times 10^{15}$ | 4.10  | 4.15        |
|         | SV   | 0.8–8           | $5.13 \times 10^3$ | 2.43       | 471 | $1.48 \times 10^{15}$ | 4.04  |             |
|         | SH   | 0.8–8           | $3.71 \times 10^3$ | 4.82       | 531 | $3.81 \times 10^{15}$ | 4.32  |             |
| KMBO    | P    | 0.5–6           | $1.59 \times 10^1$ | -          | 429 | $1.74 \times 10^{14}$ | 3.42  | 3.64        |
|         | SV   | 0.8–6           | $5.49 \times 10^2$ | -          | 468 | $3.58 \times 10^{14}$ | 3.63  |             |
|         | SH   | 0.8–6           | $4.04 \times 10^2$ | 3.54       | 675 | $3.68 \times 10^{14}$ | 3.64  |             |
| KIBK    | P    | 0.6–6           | $1.22 \times 10^2$ | -          | 303 | $1.78 \times 10^{15}$ | 4.10  | 4.15        |
|         | SV   | 0.2–7           | $2.31 \times 10^2$ | 1.60       | 884 | $1.84 \times 10^{15}$ | 4.11  |             |
|         | SH   | 0.8–7           | $3.00 \times 10^2$ | 2.48       | 773 | $2.56 \times 10^{15}$ | 4.20  |             |

**Table 2:** The parameters determined from fitting a Brune source model to the displacement spectra of each component at four stations. Components where convergence is not possible are italic. Mean magnitude estimates  $\bar{M}_W$  are calculated from values of  $M_W$  on components where convergence is achieved.

## 4. Earthquake Focal Mechanism

Calculating focal mechanisms is useful for characterising the seismicity of a region as they aid in determining the orientation of stress that leads to rupture and can help to infer the style of faulting. Here, a double-couple source mechanism is derived from the polarities of the first-arriving P-wave arrivals on the vertical components of event seismograms. This is performed on the raw velocity traces so that processing artefacts are not introduced to the arrival onsets. Clear P-wave onsets are possible at nine of the stations used. The polarities, station azimuths and take-off angles at the source are then input into the FOCMEC software package to systematically search the focal sphere for acceptable solutions (Snoke, 2003). The nodal plane fitting tolerates zero errors in polarity, which provides 15 possible solutions when a uniform search angle of  $5^\circ$  in the trend and plunge of the B axis and the slip direction are implemented.

The 15 possible fault plane solutions range in strike between N342.9°E and N004.3°E, in dip between  $60.1^\circ$  and  $81.0^\circ$  and in rake between  $-64.7^\circ$  and  $-84.8^\circ$  (Fig. 5). The mean strike, dip and rake for the event is N355.3°E,  $72.2^\circ$  and  $-76.4^\circ$  and the average azimuths and plunges of the P- and T-axes are N284.8°E,  $60.2^\circ$  and N074.8°E,  $25.6^\circ$  respectively. The source mechanism is indicative of normal faulting on a structure striking ~N-S, where the azimuth of the T-axis is oblique to the direction of maximum extension at ~N095°E (Bilham et al., 1999; Stamps et al., 2008). The proximity of the event to the mapped Wonji faults at the western edge of the caldera wall supports this as the primary nodal plane. The solution is also consistent with the general pattern of normal focal mechanisms trending N-NE along the MER (e.g., Foster & Jackson,

1998; Hofstetter & Beyth, 2003; Keir et al., 2006a), including two events occurring in the Hawassa caldera basin in 1983 and 1995 (Fig. 2b). The variability in the computed fault plane solutions is caused by the large azimuthal gaps in the station coverage to the east and west of the event, which are  $154.0^\circ$  and  $129.4^\circ$  respectively.

## 5. Discussion

We locate the earthquake on the 24th January 2016 between those provided by the NEIC and CSEM on the western edge of the Hawassa caldera, at 4.55 km depth. The earthquake locations derived by the NEIC, CSEM and in this study are all significantly distant from the Corbetti volcanic centre (15–30 km) and hence the event is unlikely to be related to volcano-tectonic processes associated with the ongoing unrest observed at Corbetti. Instead it is suggested that the earthquake is caused by slip on faults belonging to the WFB. These faults have exploited structural weaknesses originating from the collapse of the Hawassa caldera in the early Pleistocene, along its western edge. This concept is consistent with the computed source mechanism, which suggests normal faulting along a  $\sim$ N-S striking fault plane. It is evident however that with few stations to the east and west of the event location that uncertainties are present in the determined focal mechanism, due to a lack of coverage of the focal sphere. We suggest that future fault plane solutions would be better constrained with enhanced off-rift monitoring.

An earthquake in 1983 close to the eastern escarpment of the caldera basin and an event in 1995 located beneath the northwestern rim, may also be associated with slip on  $\sim$ NNE striking Wonji faults, related to Hawassa's caldera collapse (Fig. 2c). In addition to the 2016 Hawassa event, both of these events exhibited normal faulting and provide evidence that strain accumulates along the WFB at this latitude and that these structures remain seismically active. This is significant as the seismic hazard has been previously assumed to be less at this rift segment than elsewhere in the MER (Grünthal et al., 1999). We suggest that earthquakes occurring on these faults provide a significant hazard to surrounding areas.

Using four stations we determine a  $M_L$  for the event of  $4.68 \pm 0.27$ . An investigation into the relationship between  $m_b$  and  $M_W$  by Gasperini et al. (2013) has shown that  $m_b$  is a good proxy for  $M_W$  at  $m_b < 4.5$ –5, which suggests that our upper estimate of  $M_W = 4.29$  when only using FURI, is a more accurate estimate of the earthquake's size compared to when using all four. The poor spectral fits observed at the distant stations, LODK, KIBK and KMBO are likely caused by elevated rates of attenuation that suppress frequencies above  $\sim 0.8$  Hz. The emergence of mantle phases ( $P_n$ ) and uncertainties in the geometrical spreading at large ( $>200$  km) source-station offsets may also introduce uncertainties to the fitting procedure that then underestimate the spectral amplitude and hence  $M_0$  and  $M_W$  also.

## 6. Conclusions

In this paper we have relocated a significant earthquake in the MER in January 2016 using data acquired from national and global seismic networks. The location is suggestive of shallow (4.55 km depth) faulting on structures associated with the collapse of the Hawassa caldera. This is further supported by the computed source mechanism, which shows ~N-S normal slip. We calculate local and moment magnitudes of 4.68 and 4.29 using an attenuation term specific to the MER and through spectral analysis respectively.

The 2016 earthquake is the latest example that earthquakes occurring on faults associated with magma-assisted rifting in this region are capable of causing structural damage and public anxiety at local distances. In addition to the 1995  $M_W$  5.0 and 1983  $M_W$  5.1 events, this relatively shallow event highlights that precautions for future earthquakes in the region should be considered in the form of building regulations and disaster planning. Through educating the public on seismic hazard and raising awareness, it may be possible to avoid future injuries and confusion such as those experienced in Hawassa.

We therefore suggest that such outreach should be pursued by authorities on a regional and national level. Through enhanced monitoring, particularly to the east and west of the caldera, it would be possible to better refine event locations and better constrain focal mechanisms for events occurring within and around the basin. The focused monitoring of Corbetti as part of the UK NERC funded RiftVolc project is currently underway and will monitor the seismicity for five years between February 2016 and October 2017. However at present there are no plans to monitor the wider region of the Hawassa basin.

**Author contributions and declaration:** Earthquake seismograms were acquired from the Global Seismic Network and GEOFON. EH network stations are operated by the IGSSA observatory at Addis Ababa University. M.W. is funded by an Engineering and Physical Sciences Research Council (EPSRC) studentship. This research did not receive any specific grant from funding agencies in the public, commercial, or not-for-profit sectors.

## Figure Captions

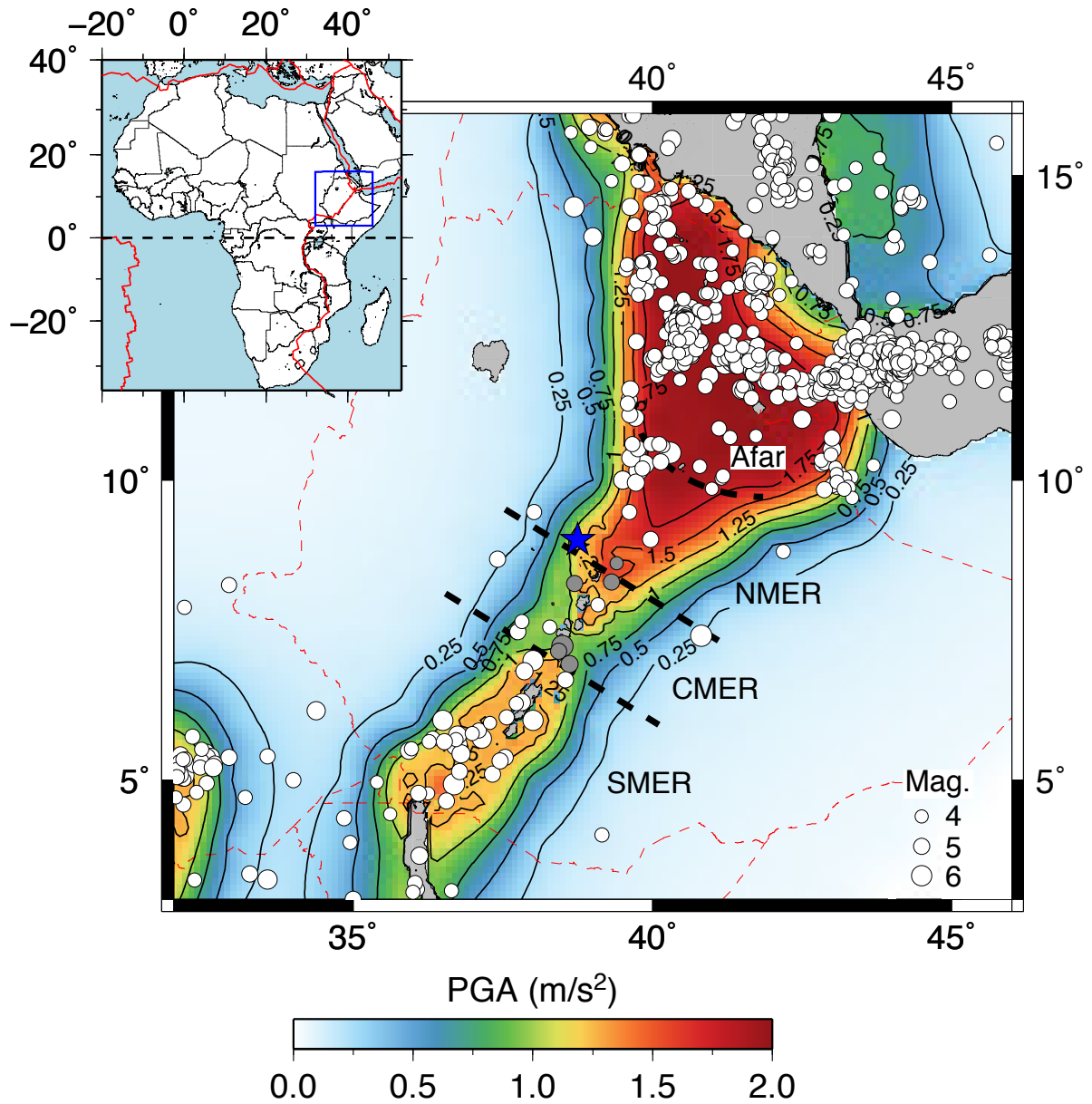


**Figure 1:** Seismic hazard map of Ethiopia and the Main Ethiopian Rift from the Global Seismic Hazard Assessment Program (after Grünthal et al., 1999). The PGA is contoured in  $0.25 \text{ m/s}^2$  increments. Earthquakes since 1900 of  $M > 4$  are white circles and sized by magnitude (International Seismological Centre, 2016). The six listed significant earthquakes in the MER are grey. Thick dashed black lines mark the boundaries of the rift segments. National borders are dashed red lines and the capital city of Addis Ababa is the blue star.

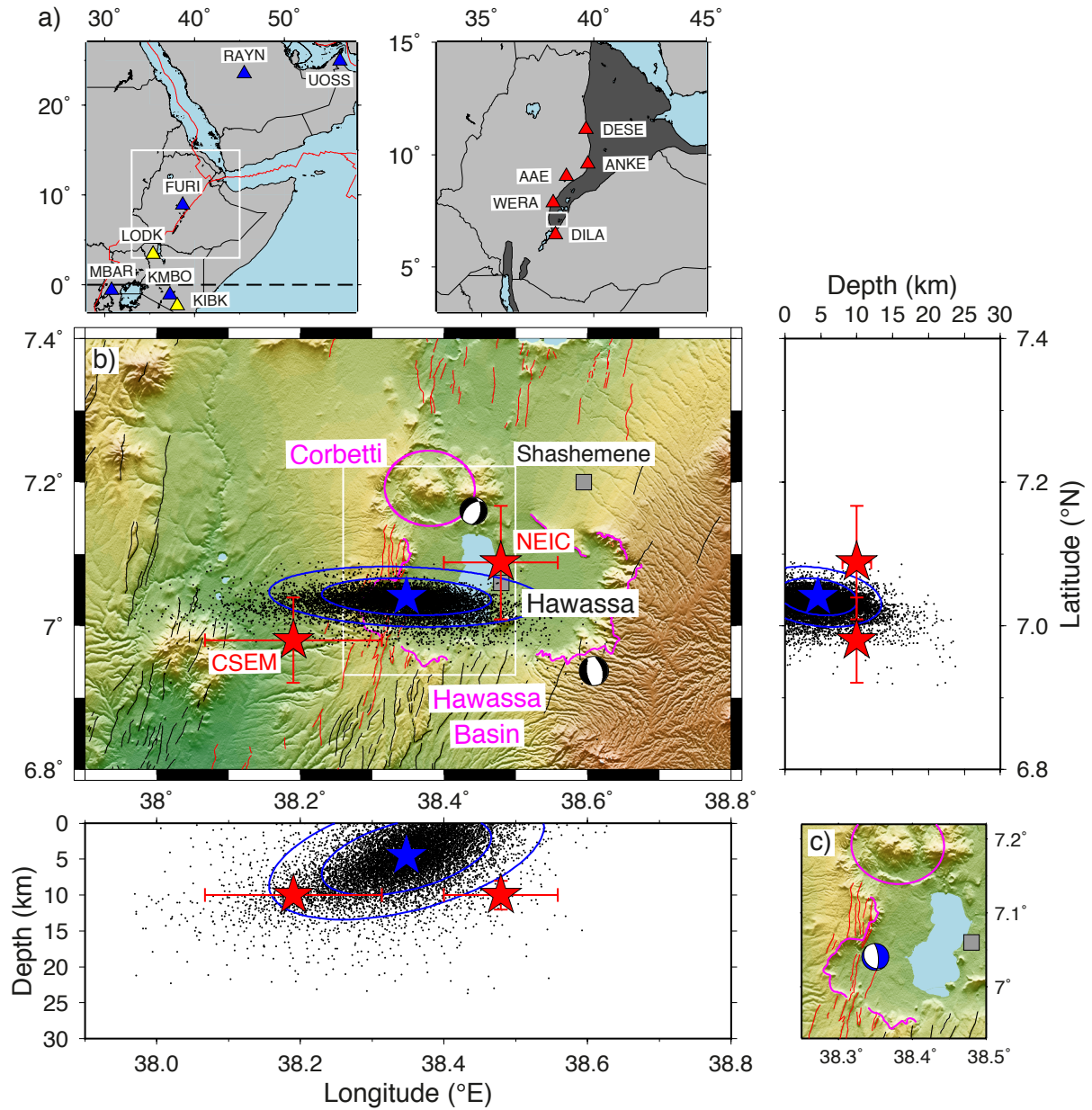


**Figure 2:** (a) The seismic stations used for analysis. Stations from the GSN, GEOFON and EH networks are blue, yellow and red triangles respectively. (b) The Hawassa earthquake location with cross-sections in depth where 0 km is sea level. The maximum probability event location is the blue star with the 68 and 95% uncertainty ellipsoids. The scatter cloud from the output PDF are black points. The locations reported by the NEIC and CSEM are red stars. Focal mechanisms for the 1995 Corbetti and 1983 Hawassa caldera events are also presented. Pink lines are the Corbetti and Hawassa caldera structures. Black and red lines are border and Wonji faults respectively. The cities of Shashemene and Hawassa are grey squares. (c) Inset of the focal mechanism for the 2016 event.

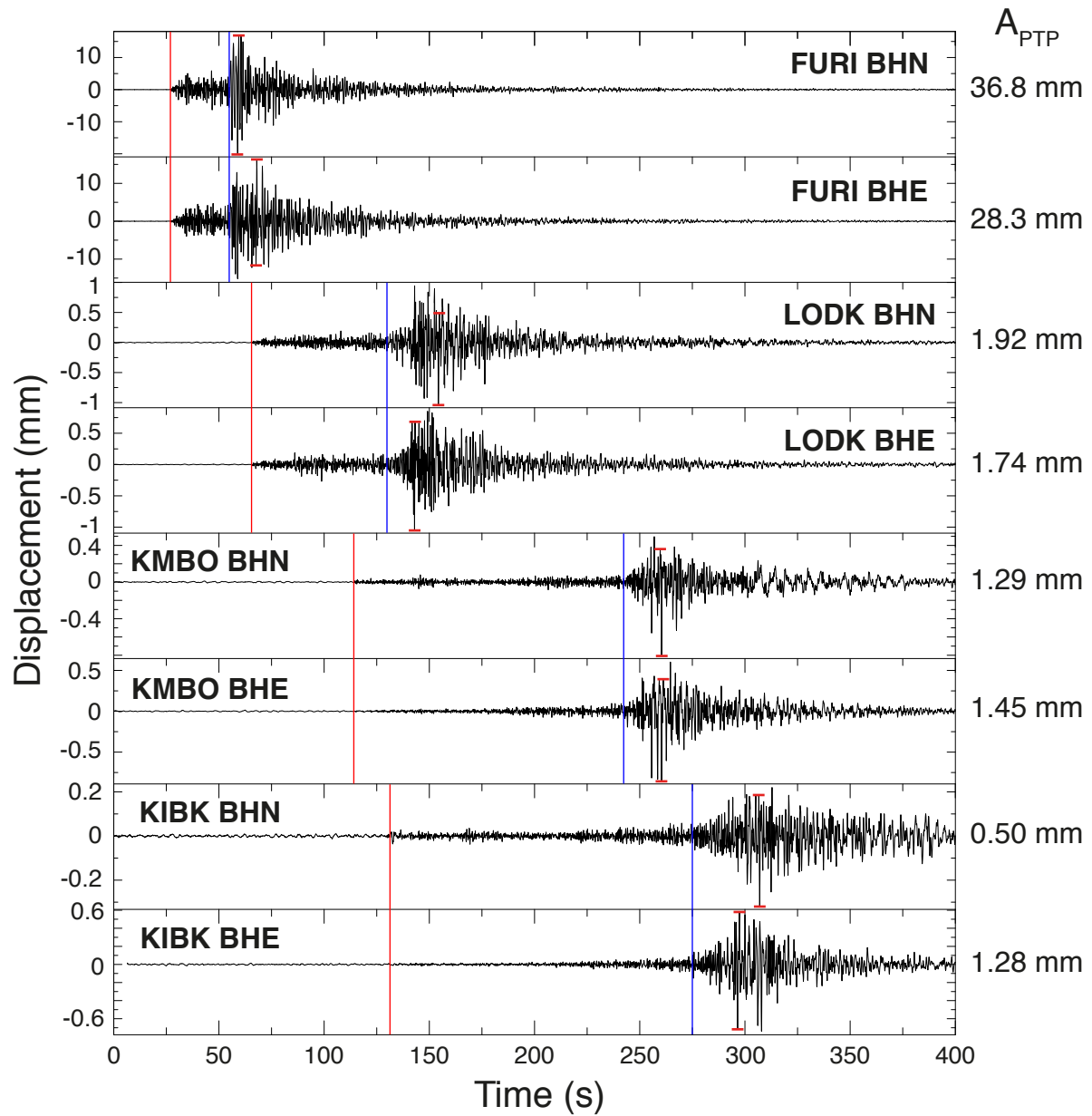


**Figure 3:** Seismograms of the Hawassa event recorded at FURI, LODK, KMBO and KIBK. The horizontal components are convolved to the response of a Wood-Anderson seismograph and the maximum peak-to-peak amplitudes are then measured (red ticks). P- and S-wave arrivals are red and blue vertical lines respectively.

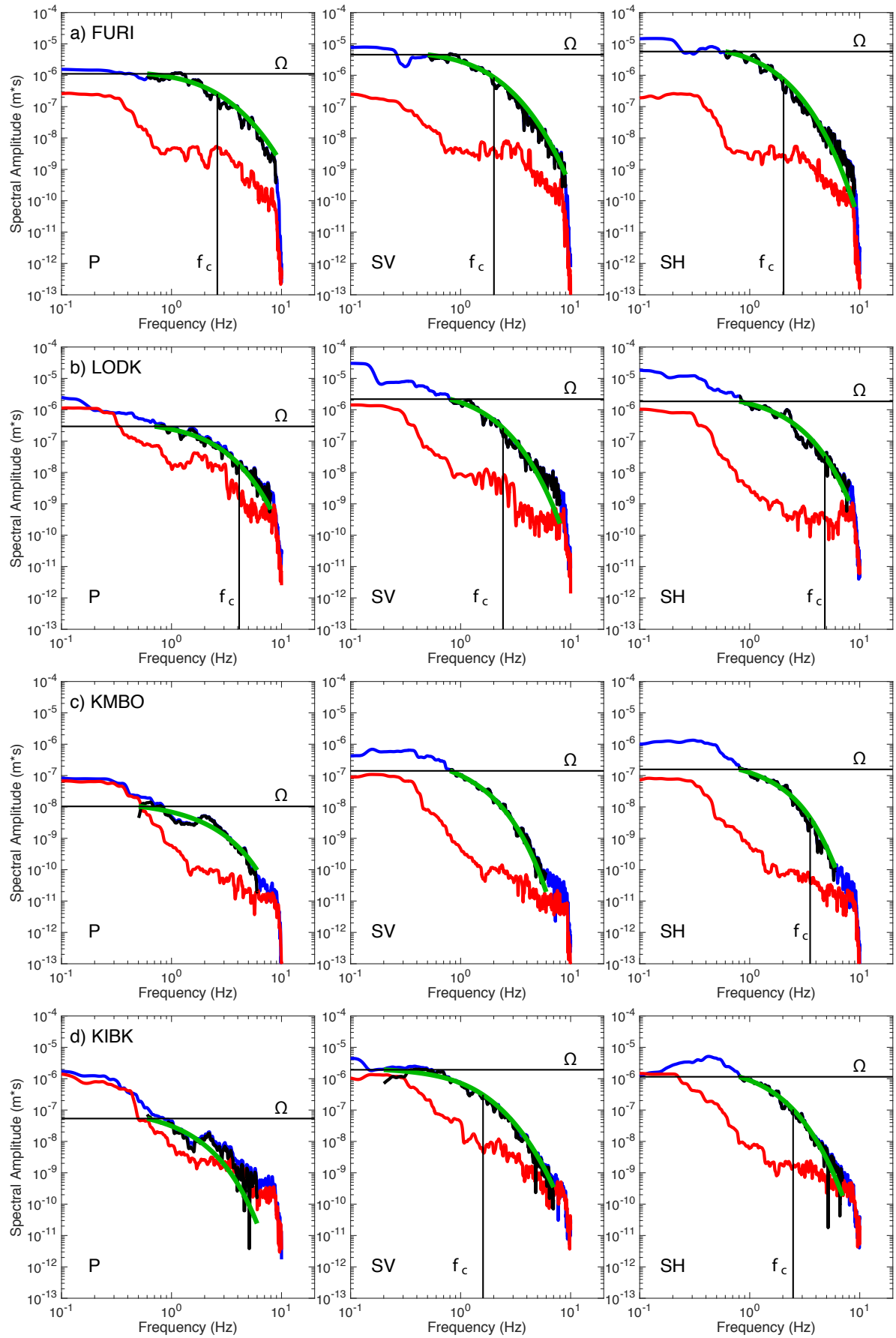


**Figure 4:** Fitting the P-, SV- and SH-wave spectra with a Brune source model at (a) FURI, (b) LODK, (c) KMBO and (d) KIBK. The spectra of the signal is blue, noise is red and the difference is black. The best fitting Brune model is the green line. The maximum spectral level,  $\Omega$  and corner frequency  $f_c$  are horizontal and vertical black lines respectively. The units of spectral amplitude are m/Hz.

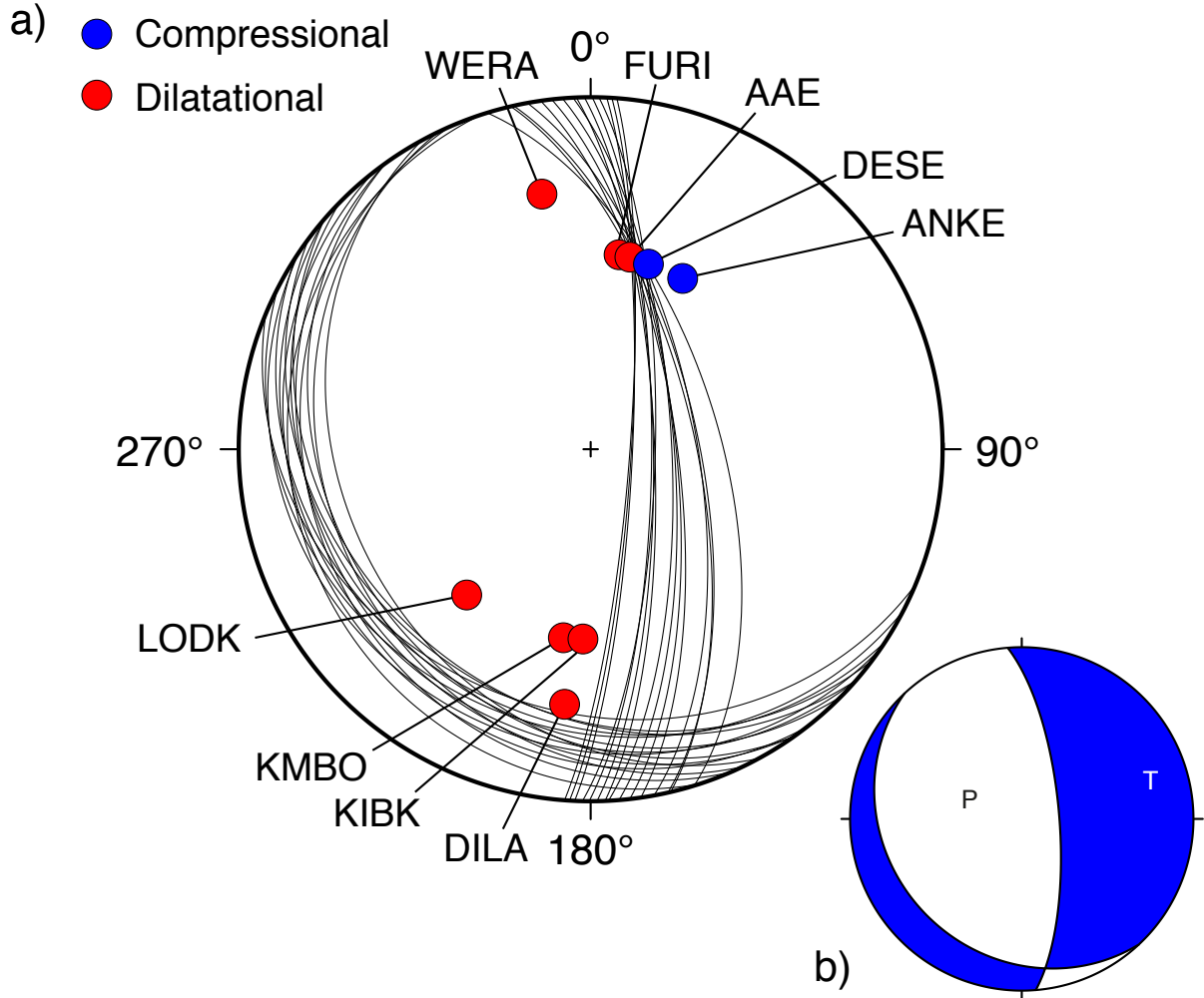


**Figure 5:** (a) Focal mechanism solutions for the Hawassa event. Blue circles indicate compressional first motions and blue circles indicate dilatational. The stations are also labelled (b) The average solution with the P and T-axes labelled.



## References

- Agostini, A., Bonini, M., Corti, G., Sani, F., & Mazzarini, F., 2011. Fault architecture in the Main Ethiopian Rift and comparison with experimental models: Implications for rift evolution and Nubia-Somalia kinematics, *Earth and Planetary Science Letters*, 301(3-4), 479–492.
- Aki, K. & Richards, P. G., 2002. *Quantitative Seismology*, University Science Books, Sausalito, California, 2nd edn.
- Asfaw, L. M., 1998. Environmental hazard from fissures in the Main Ethiopian Rift, *Journal of African Earth Sciences*, 27(3-4), 481–490.
- Biggs, J., Bastow, I. D., Keir, D., & Lewi, E., 2011. Pulses of deformation reveal frequently recurring shallow magmatic activity beneath the Main Ethiopian Rift, *Geochemistry, Geophysics, Geosystems*, 12(9), 1–11.
- Bilham, R., Bendick, R., Larson, K., Mohr, P. A., Braun, J., Tesfaye, S., & Asfaw, L., 1999. Secular and tidal strain across the Main Ethiopian Rift, *Geophysical Research Letters*, 26(18), 2789–2792.
- Boccaletti, M., Bonini, M., Mazzuoli, R., Abebe, B., Piccardi, L., & Tortorici, L., 1998. Quaternary oblique extensional tectonics in the Ethiopian Rift (Horn of Africa), *Tectonophysics*, 287(1-4), 97–116.
- Bonini, M., Corti, G., Innocenti, F., Manetti, P., Mazzarini, F., Abebe, T., & Pecskey, Z., 2005. Evolution of the Main Ethiopian Rift in the frame of Afar and Kenya rifts propagation, *Tectonics*, 24, TC1007.
- Bormann, P., Dewey, J. W., Gabsatarova, I., Gregersen, S., Gusev, A. A., Kim, W. Y., Patton, H. J., Presgrave, B. W., Ruifeng, L., Saul, J., Storchak, D., Uhrhammer, R. A., Wendt, S., Firbas, P., Havskov, J., Klinge, K., & Veith, K., 2013. Summary of Magnitude Working Group Recommendations on Standard Procedures for Determining Earthquake Magnitudes from Digital Data, Tech. rep., IASPEI.
- Brune, J. N., 1970. Tectonic stress and the spectra of seismic shear waves from earthquakes, *Journal of Geophysical Research*, 75(26), 4997–5009.
- Casey, M., Ebinger, C. J., Keir, D., Gloaguen, R., & Mohamed, F., 2006. Strain accommodation in transitional rifts: extension by magma intrusion and faulting in Ethiopian rift magmatic segments, in *The Afar Volcanic Province within the East African Rift System*, vol. 259, chap. 3, pp. 143–163, eds Yirgu, G., Ebinger, C. J., & Maguire, P. K. H., Geological Society of London, London, Special Publications.

- Chorowicz, J., Collet, B., Bonavia, F., & Korme, T., 1994. NW to NNW extension direction in the Ethiopian Rift deduced from the orientation of structures and fault slip analysis, *Geological Society of America Bulletin*, 105, 1560–1570.
- Ebinger, C. J., 2005. Continental break-up: the East African perspective, *Astronomy & Geophysics*, 46, 2.16–2.21.
- Ebinger, C. J. & Casey, M., 2001. Continental breakup in magmatic provinces: An Ethiopian example, *Geology*, 29(6), 527.
- Fantahun, A., 2016. Magnitude 4.3 Earthquake strikes Awassa, Ethiopia Observer.
- Foster, A. N. & Jackson, J. A., 1998. Source parameters of large African earthquakes: implications for crustal rheology and regional kinematics, *Geophysical Journal International*, 134(2), 422–448.
- Gasperini, P., Lolli, B., & Vannucci, G., 2013. Body-Wave Magnitude  $m_b$  Is a Good Proxy of Moment Magnitude  $M_w$  for Small Earthquakes ( $m_b < 4.5$ –5.0), *Seismological Research Letters*, 84(6), 932–937.
- Gouin, P., 1979. Earthquake History of Ethiopia and the Horn of Africa, International Development Research Centre, Ottawa, Ontario.
- Grünthal, G., Bosse, C., Sellami, S., Mayer-Rosa, D., & Giardini, D., 1999. Compilation of the GSHAP regional seismic hazard for Europe, Africa and the Middle East, *Annali di Geofisica*, 42(6), 1215–1223.
- Gutenberg, B. & Richter, C. F., 1956. Earthquake Magnitude, Intensity, Energy and Acceleration, *Bulletin of the Seismological Society of America*, 46, 105–145.
- Havskov, J. & Ottemoller, L., 2010. Routine Data Processing in Earthquake Seismology, Springer, London, UK.
- Hayward, N. J. & Ebinger, C. J., 1996. Variations in the along-axis segmentation of the Afar Rift system, *Tectonics*, 15(2), 244–257.
- Herrmann, R. B. & Kijko, A., 1983. Modeling some empirical vertical component  $L_g$  relations, *Bulletin of the Seismological Society of America*, 73(1), 157–171.
- Hofstetter, R. & Beyth, M., 2003. The Afar Depression: interpretation of the 1960–2000 earthquakes, *Geophysical Journal International*, 155, 715–732.
- Hutchison, W., 2015. Past, present and future volcanic activity at restless calderas in the Main Ethiopian Rift, Doctor of philosophy, University of Oxford.

- International Seismological Centre, 2016. On-line Bulletin, Internatl. Seis. Cent.,  
Thatcham, United Kingdom.
- Kebede, S., 2014. Geothermal Exploration and Development in Ethiopia: Country  
Update, in Short Course IX on Exploration for Geothermal Resources, p. 8, UNU-  
GTP, GDC and KenGen, Lake Bogoria and Lake Naivasha, Kenya.
- Keir, D., Ebinger, C. J., Stuart, G. W., Daly, E., & Ayele, A., 2006a. Strain  
accommodation by magmatism and faulting as rifting proceeds to breakup:  
Seismicity of the northern Ethiopian rift, *Journal of Geophysical Research*, 111(B5),  
B05314.
- Keir, D., Stuart, G. W., Jackson, A., & Ayele, A., 2006b. Local Earthquake Magnitude  
Scale and Seismicity Rate for the Ethiopian Rift, *Bulletin of the Seismological Society  
of America*, 96(6), 2221–2230.
- Kennett, B. L. N., Engdahl, E. R., & Buland, R., 1995. Constraints on seismic velocities  
in the Earth from traveltimes, *Geophysical Journal International*, 122, 108–124.
- Lomax, A., Virieux, J., Volant, P., & Berge-Thierry, C., 2000. Probabilistic earthquake  
location in 3D and layered models - Introduction of a Metropolis-Gibbs method and  
comparison with linear locations, in *Advances in Seismic Event Location*, pp. 101–  
134, eds Thurber, C. H. & Rabinowitz, N., Kluwer, Amsterdam.
- Lomax, A., Michelini, A., & Curtis, A., 2009. *Earthquake Location, Direct, Global-  
Search Methods*, Springer New York, New York, NY.
- Midzi, V., Hlatywayo, D., Chapola, L., Kebede, F., Atakan, K., Lombe, D.,  
Turyomurugyendo, G., & Tugume, F., 1999. Seismic hazard assessment in Eastern  
and Southern Africa, *Annali di Geofisica*, V42(6), 1067–1083.
- Mohr, P. A., 1967. The Ethiopian Rift System, *Bulletin of the Geophysical Observatory  
of Addis Ababa*, 11, 1–65.
- National Earthquake Information Center [NEIC], 2016. *Earthquake Information  
Bulletin*, U.S. Geological Survey, Denver, CO.
- Snoke, J. A., 2003. FOCMEC: FOCal MEChanism determinations, in *International  
Handbook of Earthquake and Engineering Seismology*, vol. 85, chap. 12, pp. 1629–  
1630, eds Lee, W. H. K., Kanamori, H., Jennings, P. C., & Kisslinger, C., Academic  
Press, San Diego.
- Stamps, D. S., Calais, E., Saria, E., Hartnady, C., Nocquet, J.-M., Ebinger, C. J., &  
Fernandes, R. M., 2008. A kinematic model for the East African Rift, *Geophysical  
Research Letters*, 35, L05304.

- 522 WoldeGabriel, G., Aronson, J. L., & Walter, R., 1990. Geology, geochronology, and rift  
523 basin development in the central sector of the Main Ethiopia Rift, Geological Society  
524 of America Bulletin, 102(4), 439–458.  
525
- 526 Wolfenden, E., Ebinger, C. J., Yirgu, G., Deino, A., & Ayalew, D., 2004. Evolution of  
527 the northern Main Ethiopian rift: birth of a triple junction, Earth and Planetary  
528 Science Letters, 224(1-2), 213–228.